IEEE Access
Multidisciplinary | Rapid Review | Open Access Journal

Date of publication xxxx 00, 0000, date of current version xxxx 00, 0000.

Digital Object Identifier 10.1109/ACCESS.2017.DOI

Identification of Islanding Events in Utility Grid with Renewable Energy Penetration Using Current Based Passive Method

NAGENDRA KUMAR SWARNKAR[1], OM PRAKASH MAHELA[2], (SENIOR MEMBER, IEEE), BASEEM KHAN[3], (MEMBER, IEEE), AND MAHENDRA LALWANI[1]

[1]Department of Electrical Engineering, Rajasthan Technical University, Kota-324010, India (swarnkar.n123@gmail.com, mlalwani.ee@gmail.com)
[2]Power System Planning Division, Rajasthan Rajya Vidyut Prasaran Nigam Ltd., Jaipur-302005, India (opmahela@gmail.com)
[3]Department of Electrical Engineering, Hawassa University, Ethiopia (baseem.khan04@gmail.com)

Corresponding author: Baseem Khan (e-mail: baseem.khan04@gmail.com).

ABSTRACT

Renewable energy (RE) generation levels are increasing in modern power systems at a fast rate due to their advantages of clean and non-exhaustible nature of energy. However, this type of generation creates technical challenges in terms of operation and control due to uncertain and un-predictable nature of generation. Islanding is an operational scenario where there is a loss of grid and RE generators continue to feed power to the local load. This has harmful effects on the RE generators and operating personal. Hence, it is expected that islanding scenario is identified in minimum time and RE generators are disconnected within $2s$ duration after island formation. This paper designed an islanding identification scheme (IDS) by designing a current islanding detection indicator (CIDI) that combines the features computed by processing the current signals, negative sequence current (NSC) and negative sequence voltage (NSV) using the Stockwell transform (ST) and the Hilbert transform (HT). Information contained by the total harmonic distortions of voltage (THD_v) and current (THD_i) is also used while designing the CIDI. Islanding and non-islanding events of category-I & II are identified and discriminated from each other by comparison of peak magnitude of CIDI with the first threshold value (FTV) and second threshold value (STV). This IDS effectively recognizes the islanding events even in the noisy environment with minimum non-detection zone (NDZ) and minimum time. The efficiency is greater than 98% even with the noise of $20dB$ SNR (signal to noise ratio). The performance of proposed IDS is better compared to IDS using discrete wavelet transform (DWT), Empirical mode decomposition (EMD), Slantlet transform & Rdigelet probabilistic neural network (RPNN), and artificial neural network (ANN). The effectiveness of IDS is validated on IEEE-13 nodes test system using MATLAB software, practical distribution network and in real time scenario by use of real time digital simulator (RTDS).

INDEX TERMS Hilbert transform; Islanding; Renewable Energy; Stockwell transform; utility grid network.

I. INTRODUCTION

RENEWABLE energy generators are installed near the load centres and excess energy is exchanged with the utility grid. Main operational consideration of these generators is the islanding scenario in which a part of the utility Network, which has loads and RE generators remains energized while it is isolated from the network of main utility grid [1]. International standards including IEEE 1547–2003, IEC 62116, IEEE 929–200, AS 4777.3-2005, UL 1741 and VDE 0126-1-1 define that RE generators should be disconnected from utility grid within $2s$ after formation of island scenario [2]. This can be achieved by the application of efficient and fast islanding detection schemes (IDS). These IDSs are classified as remote IDS and local IDS depending on the installation of devices used for measurement. Local IDSs may be passive, active and hybrid in nature. In [3],

authors presented a detailed study of active anti-islanding methods which can effectively be used for module integrated converters (MICs). These techniques are effective with high solar photovoltaic (PV) energy penetration level in the distribution grid operated at low voltages. Comparative study of these anti-islanding schemes is discussed considering the parameters such as NDZ, reduced false-detection zone, and power quality (PQ) compliance requirements. A study to investigate the impact of inverters used for grid integration of distributed-energy-resource (DER) on anti-islanding protection schemes in presented in [4]. An anti-islanding scheme using harmonic injection is designed which is effective with different penetration-levels of DERs and different conditions of islanding-networks. Passive IDSs either use variations in the system parameters or processing of the current and voltage signals by the application of signal processing techniques [5]. A passive IDS using features extracted from reactive power applying the EMD and K-means clustering is designed in [6]. It is effective to identify islanding events in a time period of two cycles with small NDZ without affecting the quality of power. Ahmad *et al.* [7], designed a passive IDS that identifies the islanding events using a voltage index. It is effective to recognize islanding events even with large power mismatches with minimum NDZ in the presence of Multi distributed generators. A multi-variable IDS using combination of features evaluated from voltage signal using ST and parameter variations are designed by authors in [8]. It effectively identifies the islanding conditions and discriminates these conditions from faulty and operational events with minimum NDZ. A hybrid IDS combining a remote detection scheme and a passive IDS is designed by the authors in [9]. It functions by usage of error rates of system parameters including the voltage and power for readjusting the generator controllers while maintaining the stability of system. It's performance is not affected by changes in the load and generation. It is effective even when faulty events are incident on the system. An IDS using information extracted from the frequency and phase angle is designed by authors in [10]. This IDS has advantages that threshold is independent of frequency and phase angle and the performance of IDS is not affected by power mismatch. In [11], authors introduced an IDS which is based on the analysis of impedance and frequency drift. This IDS is effective even when grid is weak with high inverter power rating. An empirical mode decomposition (EMD) based passive IDS which is effective for multi-distributed generators (DG) is reported in [12]. A multi-signal based IDS for solar photovoltaic (PV) inverter system using slantlet Transform and RPNN is introduced in [13]. It has eliminated the requirement of threshold. In [14], authors designed an ANN based islanding detection method which uses the samples of voltage recorded on the generator terminals.

It is observed that existing islanding detection schemes use the monitoring of variations in the parameters which include rate of changes in voltage, rate of changes in frequency, voltage THD and current THD. The reported IDSs are also designed by applying the signal processing techniques to process the voltage or current signals. Performance of these techniques can be improved by the combination of variations in the parameters with the features of current signals extracted by the application of two or more signal processing techniques. This has been considered as research objective in this paper and main contributions are detailed below:-

- A current islanding detection indicator is proposed for identification of islanding conditions and discriminating such conditions from faulty and operational events. This CIDI combines the information contained in the THD of voltage and currents, current signal, negative sequence voltage and current processed by applying ST and HT to identify the islanding events.
- This IDS is effective to identify the events and categorize these events in three categories of islanding events, non-islanding events of category-I and non-islanding events of category-II by comparing the peak magnitude of CIDI with the thresholds FTV and STV. This is achieved with minimum NDZ.
- IDS is effective to identify the events in noisy environment with high noise levels of $20dB$ SNR.
- IDS can be effectively implemented for identification of islanding condition observed on a real time distribution network where RE generators are integrated and maintain 50% RE penetration level.
- Performance of IDS is better compared to the techniques making use of EMD, Slantlet transform & RPNN, ANN and DWT in terms of minimum time for islanding identification, minimum NDz and effectiveness in the noisy scenario.

The contents are arranged in eleven sections of the paper. Introductory information and research contribution are discussed in Section I. Test utility grid network used for the study is described in the Section II. Islanding detection scheme is elaborated in Section III. Results of simulation for identifying the islanding events are detailed in Section IV. Simulation results used to recognize fault events and discriminating such conditions from islanding scenarios are detailed in Section V. Simulation results used to identify the operational events and discriminate such events from the islanding scenarios are detailed in Section VI. Categorization of islanding events and non-islanding events in different categories are discussed in the Section VII. Performance of IDS is evaluated in Section VIII. Section IX details results to validate the IDS for identification of islanding events incident on the real time distribution network and by the use of RTDS. A performance comparative study is included in Section X. The remarks of conclusion of results obtained by application of algorithm are included in Section XI.

II. UTILITY GRID WITH RENEWABLE POWER GENERATION

Proposed IDS is effectively tested on a utility grid, which is realized using IEEE-13 node test system. A wind power plant (WPP) rated at $1.5MW$ and a solar power plant (SPP) rated

at $1MW$ are integrated on node 680 of this system using transformers WPT (wind plant transformer) and SPT (solar plant transformer) respectively as described in Fig. 1. The rated capacity of the distribution system is $5MVA$ at $60Hz$ frequency and different nodes of the system are operated at two voltage levels of $4.16kV$ and $0.48kV$ [15], [16]. Hence, in this study high penetration level of RE equal to 50% is considered. Load details used for this study are available in [17], [18]. However, loads connected to different nodes are included in Table 1. Description of feeders used in this study are available in [17], [18] and feeder lengths are included in Table 2. Details of the transformer employed at different locations of test utility grid are included in Table 3. UGT represents the transformer used for interconnecting test utility grid with the large area utility grid. Distribution transformer interconnected between the nodes 633 and 634 is designated as FCT (feeder connecting transformer) and used to maintain the node 633 at voltage of $4.16kV$ and maintain the node 634 at a voltage of $0.48kV$. Voltage regulator connected between 650 and 632 nodes of test network is not used in order to investigate the maximum effect of change in voltages during the islanding scenario. An islanding realization switch (IRS) is used between the node 650 and large area utility grid to simulate an islanding event of test system. Current signals used to implement the islanding scenario are recorded on node 650 of test utility network.

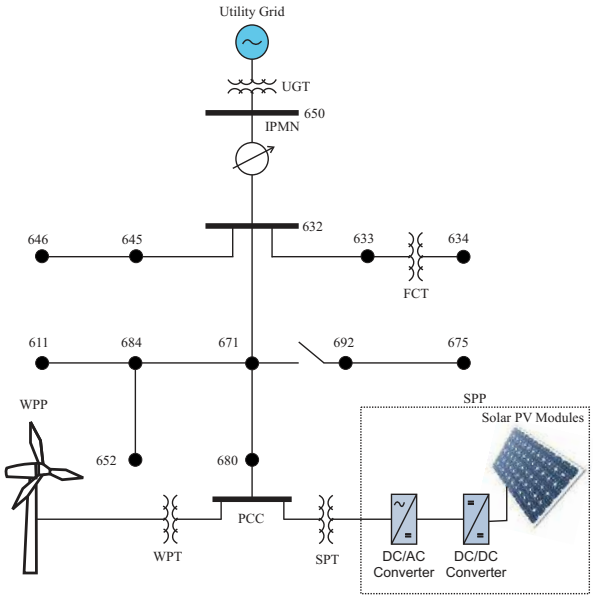

FIGURE 1. Test utility grid with renewable power generation

The WPP uses a doubly fed induction generator (DFIG) which is driven by a wind turbine. The WPP is rated at a capacity of $1.5MW$ which generates power at $575V$ and frequency of $60Hz$. Design parameters and working models of various components of WPP including DFIG, wind turbine, drive train system, and converters used in this study are available in [19], [20]. Nominal wind speed of $11m/s$ is considered in this study.

TABLE 1. Quantum of Loads Connected at Different Nodes of Test Utility Grid

Node	Quantum and Type of Load			Capacitor bank (kVAr)
	kW	kVAr	Type	
634	400	290	$3-\phi$	
645	170	125	$1-\phi$	
646	230	132	$1-\phi$	
652	128	86	$1-\phi$	
671	1255	718	$3-\phi$	
675	843	462	$3-\phi$	600
692	170	151	$1-\phi$	
611	170	80	$1-\phi$	100
632-671*	200	116	$3-\phi$	

$*$ Distributed load is considered as lumped load placed at middle of line connected between nodes 632-671.

TABLE 2. Length of Feeders

First Node	Second Node	Line length (m)
632	645	152.40
632	633	152.40
633	634	0
645	646	91.44
650	632	609.60
684	652	243.84
632	671	609.60
671	684	680
671	692	0
684	611	91.44
692	675	152.40

Solar energy generation is realized by the use of a solar photovoltaic plant (SPP) having a capacity of $1MW$. The photovoltaic (PV) arrays used in the SPP generate power of $1MW$ at DC voltage of $273.5V$. This is deemed input for the DC-DC boost converter, which increase the voltage level to $500V$. This DC power at $500V$ is given as input to the inverter that converts the DC power to 3-phase AC power rated at $260V$. SPT transformer increases the voltage level from $260V$ to $4.16kV$. Design configuration and design parameters of SPP used in this study are available in [21], [22].

III. PROPOSED ISLANDING DETECTION SCEHEME

Design of proposed islanding detection scheme (IDS) is described in this section. A flowchart indicating all the steps of IDS is described in Fig. 2. Descriptions of all steps of IDS are provided in below subsections.

A. STOCKWELL FACTOR

The current signals captured on node 650 during an event are processed using the Stockwell transform (ST) with sampling frequency $3.84kHz$ and output matrix with absolute values (STOM) is obtained. All the elements of every column are summed up and assigned the name ST summation factor (STSF) which is described below:-

$$STSF = sum(STOM) \tag{1}$$

Compute Stockwell transform maximum magnitude factor (STMMF) by finding the maximum value of every column of

This article has been accepted for publication in a future issue of this journal, but has not been fully edited. Content may change prior to final publication. Citation information: DOI 10.1109/ACCESS.2021.3092971, IEEE Access

TABLE 3. Details of Transformer used in Test Utility System

Transformer	MVA	kV-High	kV-Low	HV Winding		LV Winding	
				R(Ω)	X(Ω)	R(Ω)	X(Ω)
UGT	10	115	4.16	29.095	211.60	0.1142	0.8306
FCT	5	4.16	0.48	0.3807	2.7688	0.0510	0.0042
WPT	5	4.16	0.575	0.3807	2.7688	0.0510	0.0042
SPT	0.1	4.16	0.260	0.1730	195.70	0.0007	0.7645

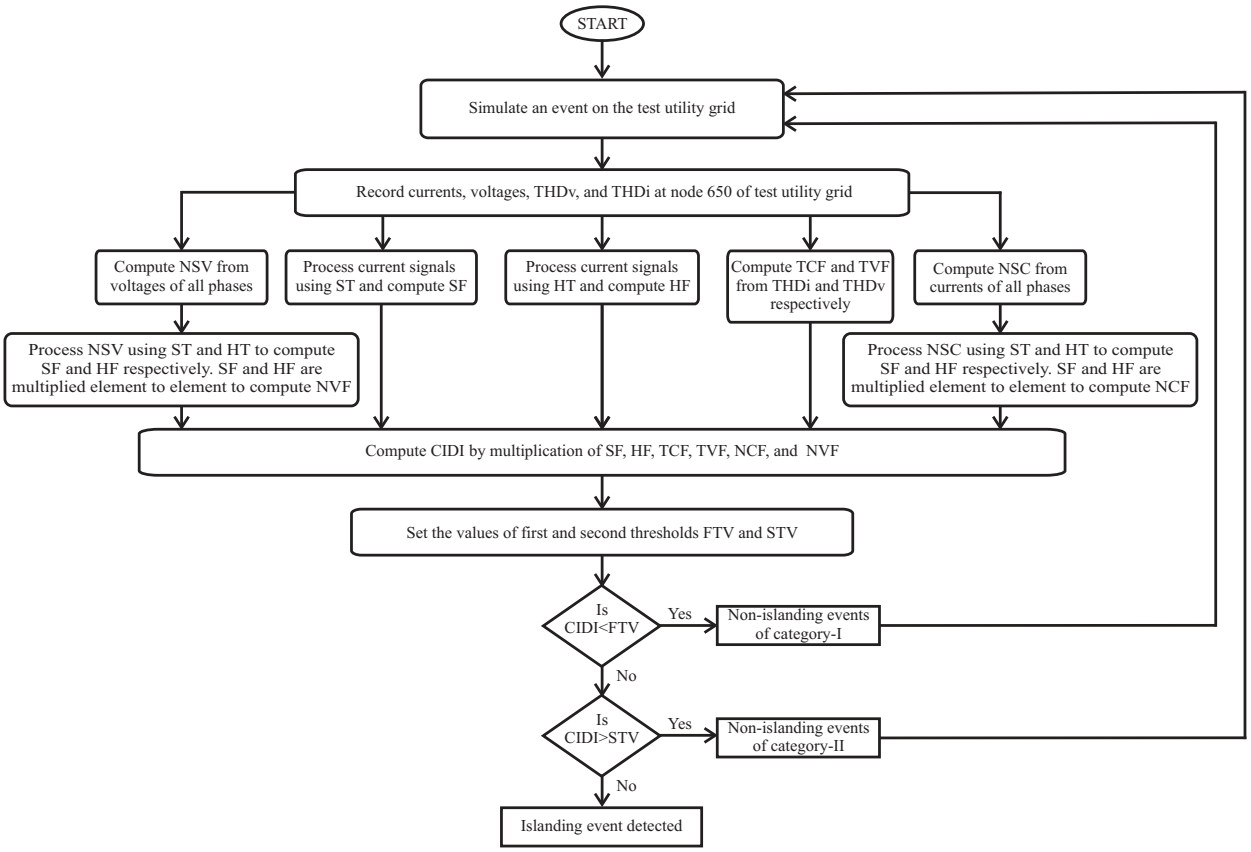

FIGURE 2. Flow scheme of current based islanding detection scheme

STOM as detailed below:-

$$STMMF = max(STOM) \tag{2}$$

Compute Stockwell transform median factor (STMF) by taking median of the matrix STOM as detailed below:

$$STMF = median(STOM) \tag{3}$$

Multiply the STSF, STMMF and STMF element to element to compute SF as detailed below:

$$SF = STSF \times STMMF \times STMF \times WSF \tag{4}$$

Here, WSF indicates the weight factor for SF and it is considered equal to 10000 for this study.

1) Stockwell Transform

The ST is considered as expansion of the continuous Wavelet transform (CWT) and effective to extract information contained in the phase spectrum and amplitude of the current signal. This is achieved by modification in phase of mother wavelet of CWT. Further, ST can also be derived from the STFT using Gaussian window function. ST has a property that if window is wide in time domain then it gives better frequency resolution where low frequencies are available. For narrow window, it gives good time resolution for high frequencies. Discrete version of ST is derived from Fast Fourier Transform (FFT) and convolution theorem. STFT of current signal *i(t)* can be formulated by below detailed formulation [23]:-

$$STFT(\tau, f) = \int_{-\infty}^{\infty} i(t)g(\tau - t)e^{-j2\pi ft}dt \tag{5}$$

where τ: spectral localization time; f: Fourier frequency; $g(t)$: window function. By replacing window function $g(t)$ by a Gaussian function, ST is derived. Gaussian window function is described below [1]:-

This article has been accepted for publication in a future issue of this journal, but has not been fully edited. Content may change prior to final publication. Citation information: DOI 10.1109/ACCESS.2021.3092971, IEEE Access

$$g(t) = \frac{|f|}{\sqrt{2\pi}} e^{-\frac{f^2 t^2}{2}} \tag{6}$$

Hence, ST is formulated by below detailed relation.

$$STOMC(\tau, f) = \int_{-\infty}^{\infty} i(t) \frac{|f|}{\sqrt{2\pi}} e^{-\frac{f^2(\tau - t)^2}{2}} e^{-j2\pi f t} dt \tag{7}$$

Here, STOMC is the output matrix every element of which are complex in nature. The STOMC contains the information of both the frequency as well as amplitude of current. Absolute values matrix STOM is evaluated from output of STOMC, obtained in above equation, as detailed below:-

$$STOM = abs(STOMC) \tag{8}$$

Different ST based factors used for the design of CIDI are computed from this STOM matrix.

B. HILBERT FACTOR

The current signals (I) are processed using the Hilbert transform (HT) and absolute values of output are computed and assigned the name Hilbert factor (HF).

$$HF = abs(hilbert(I)) \tag{9}$$

1) Hilbert Transform

Processing of current signals using the Hilbert Transform (HT) provides information pertaining to spectral components and time-frequency-energy contents of the current signal. This information is effective to recognize the islanding and non-islanding scenarios. HT is efficient in identification of frequencies available for short time and amplitude of current which is effective in identification of islanding and non-islanding scenarios. Following relation is used to process current signals using the HT [24].

$$HT = \frac{1}{\pi} PV \int_{-\infty}^{\infty} \frac{I(\tau)}{t - \tau} d\tau \tag{10}$$

where, PV, t, τ are Cauchy's principle value integral, time and time period respectively. HF is computed by computing absolute magnitudes of the HT.

$$HF = abs(HT) \tag{11}$$

The Cauchy's principal value integral (PV) of a function f(x) that becomes infinite at an interior point $x = x_0$ of the interval of integration (a, b) is the limit as defined by the below detailed relation [25].

$$PV \int_a^b f(x)dx = \lim_{\varepsilon \to 0} \left(\int_a^{x_0 - \varepsilon} + \int_{x_0 + \varepsilon}^b \right) f(x)dx \tag{12}$$

where $0 < \varepsilon \leqslant min(x_0 - a, b - x_0)$. This integral is denoted by placing PV in-front of the usual integral sign.

C. CURRENT THD FACTOR

THD of current signals recorded during the islanding events and non-islanding events is computed. This is considered as the THD current factor (TCF) for designing the CIDI.

D. VOLTAGE THD FACTOR

THD of voltage signals recorded during the islanding events and non-islanding events is computed. This is considered as the THD voltage factor (TVF) for designing the CIDI.

E. NEGATIVE SEQUENCE CURRENT FACTOR

Negative sequence current (NSC) is computed from the current signals corresponding to all the three phases recorded at the node 650 of test utility grid using the following relation.

$$I_0 = \frac{I_1 + I_2 + I_3}{3} \tag{13}$$

here, I_0: negative sequence current; I_1, I_2, and I_3 represent the current associated to phases-A, B and C in respective sequence. NSC is processed applying the ST and HT to compute the SF and HF using the equations (4) and (9) respectively. These SF and HF for the NSC are multiplied element to element for computing the Negative sequence current factor (NCF).

F. NEGATIVE SEQUENCE VOLTAGE FACTOR

Negative sequence voltage (NSV) is computed from the voltage signals corresponding to all the three phases recorded at the node 650 of test utility grid using the following relatiom.

$$V_0 = \frac{V_1 + V_2 + V_3}{3} \tag{14}$$

here, V_0: negative sequence voltage; V_1, V_2, and V_3 represent the voltage associated to phases-A, B and C in respective sequence. NSV is processed applying the ST and HT to compute the SF and HF using the equations (4) and (9) respectively. These SF and HF for the NSV are multiplied element to element for computing the Negative sequence voltage factor (NVF).

G. CURRENT ISLANDING DETECTION INDICATOR

The current islanding detection indicator (CIDI) is calculated using element to element multiplication of factors including SF, HF, TCF, TVF, NCF, NVF and current weight factor (CWF) as described below.

$$CIDI = SF \times HF \times TVF \times TCF \times NCF \times NVF \times CWF \tag{15}$$

Here, CWF is considered equal to 10^{16}.

Two threshold magnitudes are considered to discriminate the events of islanding from non-islanding events. First threshold value (FTV) is considered equal to 1000 and second threshold value (STV) is considered equal to 2×10^{12}. These magnitudes of FTV and STV are selected by testing

This article has been accepted for publication in a future issue of this journal, but has not been fully edited. Content may change prior to final publication. Citation information: DOI 10.1109/ACCESS.2021.3092971, IEEE Access

the algorithm on 160 data in the noise free and noisy environment of $20dB$ SNR. This data is obtained by varying the parameters such as fault impedance, fault incidence angle, incidence angle of islanding, different scenarios of RE generation, different scenarios of load generation balance etc. If the peak magnitude of CIDI is observed between the STV and FTV then the event incident on the test utility grid is islanding in nature. For non-islanding events included in category-I, the peak magnitude of CIDI is below the FTV. The symmetrical fault events (LLL or LLLG fault events), unsymmetrical fault events without involving ground (LL fault) and operational events are included in the non-islanding events of the category-I. For the non-islanding events included in category-II, the peak magnitude of CIDI is above the STV. The un-symmetrical fault event including ground (LLG fault event) is included in the non-islanding events of the category-II.

The proposed CIDI is based on identification of distortions in the current waveforms at the time of islanding event. Hence, CIDI can be used irrespective of the type of power converter, type of control algorithm used for the converters, nature of RE generators, penetration level of RE in the utility grid.

IV. IDENTIFICATION OF ISLANDING EVENTS: SIMULATION RESULTS

Results of simulation for identification of islanding events with availability of generation from both wind and solar power, only wind power generation and only solar power generation are discussed in this section. All steps included in implementation of the proposed IDM for identification of islanding events incident in the availability of generation from both wind and solar power plants are described in detail.

A. IDENTIFICATION OF ISLANDING EVENT WITH GENERATION FROM BOTH WIND AND SOLAR POWER PLANTS

This subsection describes all the steps used in implementation of the proposed IDS with availability of generation from both WPP and SPP. Test utility grid is simulated considering $1.5MW$ generation from WPP and $1MW$ generation from the SPP. The IRS switch is opened at 6^{th} cycle $(0.1s)$ and islanding event is realized with availability of generation from both WPP and SPP. Current signals associated with the three phases are recorded at the bus node 650 of test network. These current signals are decomposed by application of ST to compute SF described in Fig. 3 (a). The current signals are decomposed using the HT to compute HF which is illustrated in Fig. 3 (b). The TCF and TVF are computed from the THD of currents and voltages recorded at the node 650 of test utility grid and illustrated in Fig. 3 (c) and (d) respectively. NSC is computed from the currents associated with all the phases and processed using the ST and HT to compute the negative sequence current factor (NCF) illustrated in Fig. 3 (e). NSV is computed from the voltages associated to all the phases and decomposed using ST and HT to compute the negative sequence voltage factor described in Fig. 3 (f). It is viewed from Fig. 3 that magnitudes of the SF, HF, NCF, NVF, TCF and TVF changes due to the incidence of Islanding event. Fig. 3 (a) details that high magnitude peak is observed at the instant of islanding occurrence. However, HF first increases due to incidence of islanding and subsequently has decreased as detailed in Fig. 3 (b). It is perceived from the Fig. 3 (c) that magnitude of TCF has increased at moment of islanding occurrence. Magnitude of TVF increases due to incidence of islanding as detailed in Fig. 3 (d). Magnitude of the NCF has increased due to incidence of the islanding as depicted in Fig. 3 (e). However, this increase in magnitude is centralized with the moment of islanding incidence and rise in magnitude is relatively low. Fig. 3 (f), it is established that variations of NVF are close to the variations of NCF. Further, the NCF and NVF will become more prominent during unsymmetrical scenario. Individual application of these factors is not much effective for identifying the islanding scenarios and discriminating these scenarios from the non-islanding events. A CIDI is designed by combining the merits of all these factors that effectively recognize the islanding scenarios and discriminates these conditions from non-islanding events of category-I & II.

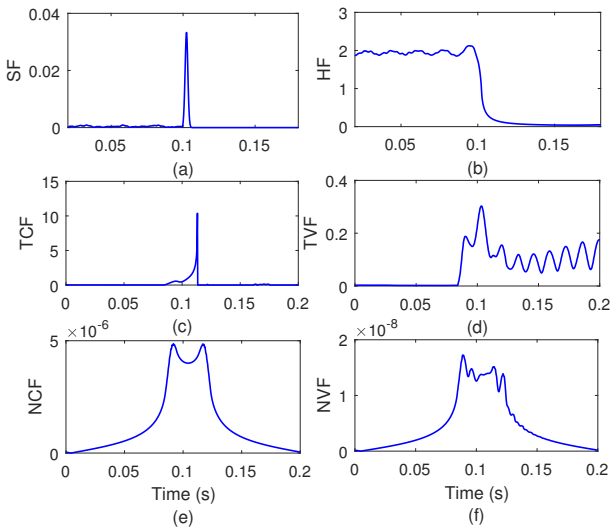

FIGURE 3. Identification of islanding scenario with availability of both WPP and SPP (a) Stockwell factor (b) Hilbert factor (c) current THD factor (d) voltage THD factor (e) negative sequence current factor (f) negative sequence voltage factor

The current signal associated with phase-A captured on node 650 of test utility grid during the scenario of islanding with availability of generation from both WPP and SPP is described in Fig. 4 (a). This is perceived that magnitude of current has decreased at instant of occurrence of islanding condition. The current signal is processed applying the proposed IDS and CIDI is evaluated which is illustrated in Fig. 4 (b). It is viewed that peak magnitude of CIDI (3.92×10^4) is greater compared to FTV and lower compared to STV. Hence, peak magnitude falling between the range of FTV and STV indicates the occurrence of islanding scenario with

This article has been accepted for publication in a future issue of this journal, but has not been fully edited. Content may change prior to final publication. Citation information: DOI 10.1109/ACCESS.2021.3092971, IEEE Access

availability of generation from both WPP and SPP. Computational time taken to identify the islanding event with SPP and WPP is tabulated in Table 4 which is less than $10ms$.

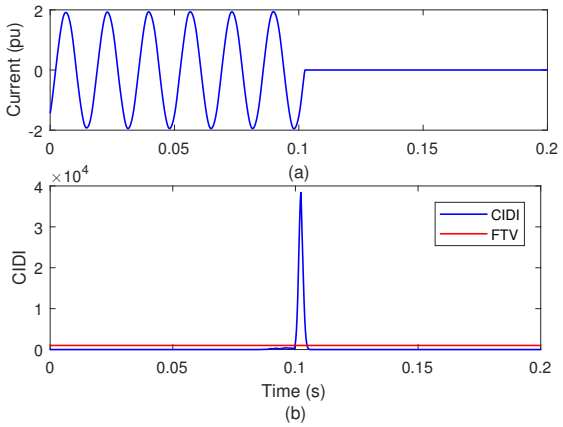

FIGURE 4. Identification of islanding event with availability of generation from both WPP and SPP (a) current associated to phase-A (b) current islanding detection indicator

TABLE 4. Computational Time Involved in Recognition of Islanding and Non-islanding Events

S. No.	Type of Event	Time (ms)
1	Identification of islanding scenario with both WPP & SPP	7.37033
2	Identification of islanding scenario with WPP	8.39376
3	Identification of islanding scenario with SPP	8.06700
4	Identification of LG fault event	5.93145
5	Identification of LLG fault event	9.69184
6	Identification of LL fault event	7.59562
7	Identification of LLLG fault event	7.98783
8	Identification of WPP outage event	5.82771
9	Identification of SPP Outage event	8.07743
10	Identification of SPP & WPP Outage event	9.31447
11	Identification of SPP & WPP Grid Synchronization event	6.78882
12	Identification of Capacitor switching event	6.60980
13	Identification of Load switching event	8.97631

1) Determination of Non Detection Zone

The operational zone where event of islanding is not identified by the IDS is considered as non-detection zone (NDZ) for the IDS. This zone is identified due to mismatch between the generated power and power consumed by loads. It is identified considering the power mismatch between active power generated and consumed by loads at various voltage levels. Formulation reported in [26] is used to compute active power mismatch as detailed below:-

$$\Delta P = 3V \times I - 3(V + \Delta V) \times I = -3\Delta V \times I \quad (16)$$

here, $V = 4.16kV$ is system voltage and I is current. Range considered for estimation of NDZ varies from $0.88pu$ to $1.1pu$. Mismatch in active power is achieved by changing the power generated by WPP & SPP. Various conditions of power mismatch and voltages are provided in Table 5. In this table, the conditions of ΔP and V corresponding to which the islanding event is recognized are indicated by IER (islanding event recognized). The limits of NDZ were the islanding event is not recognized is indicated by $IENR$ (islanding not recognized). The NDZ range of IDS in terms of power mismatch and voltages is given as (a) ΔP = -$5kW$ to $\Delta P = 5kW$ at $1.0pu$ voltage; (b) V = $0.95pu$ to V = $1.1pu$ at $\Delta P = 0kW$. Power mismatch ΔP is considered positive if power generated in the island network is higher compared to load connected to this network. Conversely, if power generated in the island network is lower compared to load connected to this network then power mismatch ΔP is considered negative. During normal operating conditions, power will not be exchanged with utility network if power mismatch is zero and for non-zero conditions of power mismatch the power will be exchanged with utility network depending on the load generation balance in the network.

B. DETECTION OF ISLANDING EVENT WITH WPP

The SPP integrated at node 680 of test utility grid is kept disconnected and WPP of capacity $1.5MW$ is kept connected to test utility grid and IRS is opened at 6^{th} cycle ($0.1s$) to simulate islanding event with generation from the WPP only. The current signal associated to phase-A measured on node 650 of test grid during scenario of islanding with generation from WPP only is processed using the proposed IDS and CIDI is computed, which is detailed in Fig. 5. It is viewed that peak value of CIDI (3.98×10^4) is greater compared to FTV and lower compared to STV, Hence, peak magnitude falling between the range of FTV and STV indicate the occurrence of islanding condition with generation from WPP only. Computational time taken to identify the islanding event with WPP is tabulated in Table 4 that is less than $10ms$.

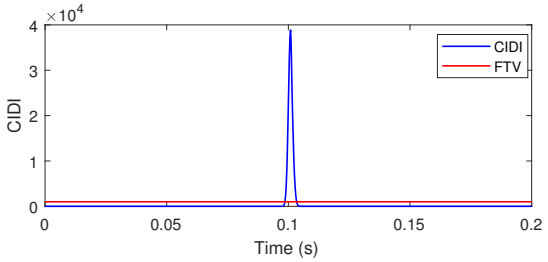

FIGURE 5. CIDI associated to scenario of islanding in the presence of WPP

C. DETECTION OF ISLANDING EVENT WITH SPP

The WPP integrated at node 680 of test grid is kept disconnected and SPP of capacity $1MW$ is kept connected to the test utility grid and IRS is opened at 6^{th} cycle ($0.1s$) to simulate islanding scenario with generation from the SPP only. The current signal associated with phase-A captured on node 650 of test grid during event of islanding in the availability

This article has been accepted for publication in a future issue of this journal, but has not been fully edited. Content may change prior to final publication. Citation information: DOI 10.1109/ACCESS.2021.3092971, IEEE Access

TABLE 5. Non-Detection Zone of Current Based IDS

ΔP	Voltage (pu)													
(kW)	.88	0.89	0.90	0.91	0.92	0.93	0.94	0.95	0.96	0.97	0.98	0.99	1.0	1.1
8	IER	IER	IER	IER	IER	IER	IER	IER	IER	IER	IER	IER	IER	IER
7	IER	IER	IER	IER	IER	IER	IER	IER	IER	IER	IER	IER	IER	IER
6	IER	IER	IER	IER	IER	IER	IER	IER	IER	IER	IER	IER	IER	IER
5	IER	IER	IER	IER	IER	IER	IER	IER	IER	IER	IER	IER	IENR	IER
4	IER	IER	IER	IER	IER	IER	IER	IER	IER	IER	IER	IENR	IENR	IENR
3	IER	IER	IER	IER	IER	IER	IER	IER	IER	IER	IENR	IENR	IENR	IENR
2	IER	IER	IER	IER	IER	IER	IER	IER	IER	IENR	IENR	IENR	IENR	IENR
1	IER	IER	IER	IER	IER	IER	IER	IER	IENR	IENR	IENR	IENR	IENR	IENR
0	IER	IER	IER	IER	IER	IER	IER	IENR	IENR	IENR	IENR	IENR	IENR	IENR
-1	IER	IER	IER	IER	IER	IER	IER	IER	IENR	IENR	IENR	IENR	IENR	IENR
-2	IER	IER	IER	IER	IER	IER	IER	IER	IER	IENR	IENR	IENR	IENR	IENR
-3	IER	IER	IER	IER	IER	IER	IER	IER	IER	IER	IENR	IENR	IENR	IENR
-4	IER	IER	IER	IER	IER	IER	IER	IER	IER	IER	IER	IENR	IENR	IENR
-5	IER	IER	IER	IER	IER	IER	IER	IER	IER	IER	IER	IER	IENR	IER
-6	IER	IER	IER	IER	IER	IER	IER	IER	IER	IER	IER	IER	IER	IER
-7	IER	IER	IER	IER	IER	IER	IER	IER	IER	IER	IER	IER	IER	IER
-8	IER	IER	IER	IER	IER	IER	IER	IER	IER	IER	IER	IER	IER	IER

of SPP only is processed using the proposed IDS and CIDI is computed, which is described in Fig. 6. It is viewed that peak magnitude of CIDI (5.42×10^4) is greater compared to FTV and lower compared to STV. Hence, peak magnitude falling between the range of FTV and STV indicates the incidence of islanding event in the presence of SPP. Computational time taken to identify the islanding event with SPP is tabulated in Table 4, which is less then, $10ms$.

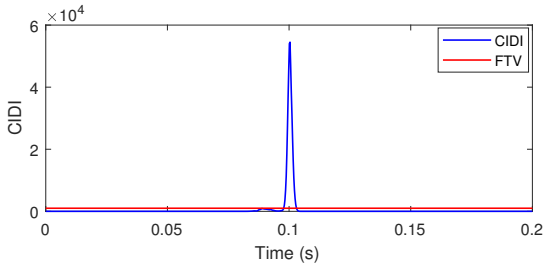

FIGURE 6. CIDI associated to the event of islanding in the presence of SPP

V. TESTING OF IDM DURING FAULTY EVENTS: SIMULATION RESULTS

This simulation results for testing of IDS to recognize the faulty conditions and discriminate such conditions from the islanding events are discussed in this section.

A. TESTING OF IDM DURING SYMMETRICAL FAULTY CONDITION

Three phase symmetrical faults involving ground (LLLG) is simulated on bus 646 of test utility network at 6^{th} cycle ($0.1s$). The current signal associated with phase-A captured on node 650 of test utility network during the conditions of LLLG fault is captured and detailed in Fig. 7 (a). It is viewed that due to the occurrence of fault, the current magnitude has increased. This current signal is processed applying the IDS and CIDI is evaluated which is illustrated in Fig. 7 (b). It is perceived that peak value of CIDI (1.63×10^{-53}) is lower compared to FTV. Hence, peak magnitude of CIDI lower compared to FTV indicates that the LLLG fault event is related to non-islanding events of category-I. Computational time taken to identify the LLLG fault event is tabulated in Table 4, which is less than $10ms$. Hence, LLLG fault event is identified and discriminated from the islanding events.

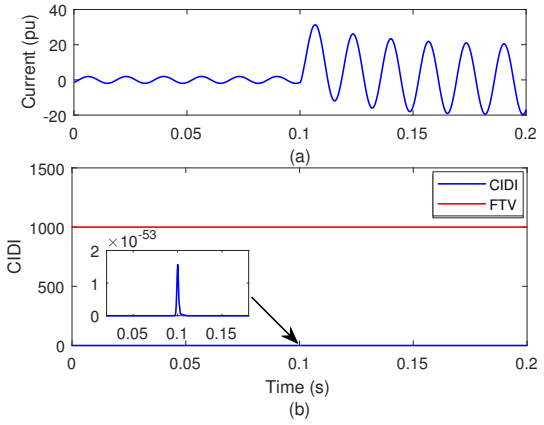

FIGURE 7. Identification of LLLG fault event (a) current signal associated to phase-A (b) current islanding detection indicator

B. TESTING OF IDM DURING UNSYMMETRICAL FAULTY CONDITION

This section details the simulation results for testing of IDS to identify the unsymmetrical faulty events and discriminate these events from the islanding events.

1) Unsymmetrical Fault involving Ground

A phase to ground (LG) un-symmetrical fault is simulated on node 646 of test utility grid at the 6^{th} cycle ($0.1s$). The current signal associated with phase-A captured on node 650 of test grid during the event of LG fault is recorded and illustrated in Fig. 8 (a). It is viewed that due to occurrence of LG fault the current magnitude has increased. This current

This article has been accepted for publication in a future issue of this journal, but has not been fully edited. Content may change prior to final publication. Citation information: DOI 10.1109/ACCESS.2021.3092971, IEEE Access

signal is decomposed using the IDS and CIDI is computed, which is illustrated in Fig. 8 (b). It is inferred that peak magnitude of CIDI (1.82×10^{17}) is higher compared to STV. Hence, peak magnitude of CIDI higher compared to STV indicates that the LG fault event is related to non-islanding events of category-II. Computational time taken to identify the LG fault event is tabulated in Table 4, which is less than $10ms$. Hence, LG fault event is identified and discriminated from the islanding events.

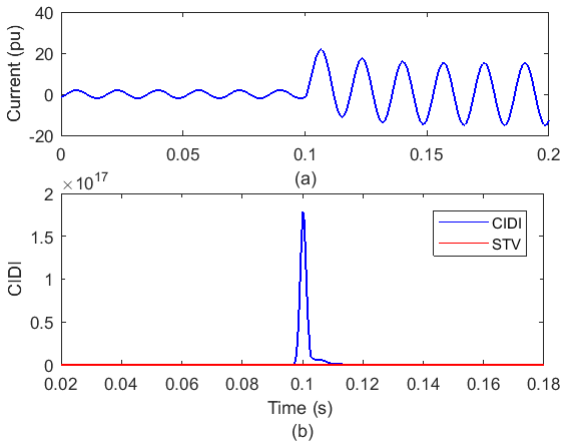

FIGURE 8. Identification of LG fault event (a) current signal associated to phase-A (b) current islanding detection indicator

Two phases to ground (LLG) un-symmetrical fault is simulated on bus 646 of test utility network at 6^{th} cycle ($0.1s$). The current signal associated with phase-A recorded on node 650 of test grid during the event of LLG fault is processed using the proposed IDS and CIDI is computed, which is described in Fig. 9. It is viewed that peak magnitude of CIDI (1.24×10^{17}) is higher compared to STV. Hence, peak magnitude of CIDI higher compared to STV indicates that the LG fault event is related to non-islanding events of category-II. Computational time taken to identify the LG fault event is tabulated in Table 4, which is less than $10ms$. Hence, LG fault event is identified and discriminated from the islanding events.

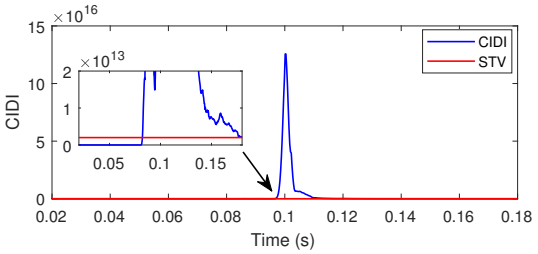

FIGURE 9. Current islanding detection indicator during LLG fault event

2) Unsymmetrical Fault without Involvement of Ground

Two phase (LL) un-symmetrical faulty event is simulated on bus 646 of test utility network at 6^{th} cycle ($0.1s$). The current signal associated with phase-A captured on bus 650 of test grid during the event of LL fault is processed using the proposed IDS and CIDI is computed, which is described in Fig. 10. It is viewed that peak magnitude of CIDI (2×10^{-33}) is lower compared to FTV. Hence, peak magnitude of CIDI lower compared to FTV indicates that the LL fault event is related to non-islanding events of category-I. Computational time taken to identify the LG fault event is tabulated in Table 4 that is less than $10ms$. Hence, LL fault event is identified and discriminated from the islanding events.

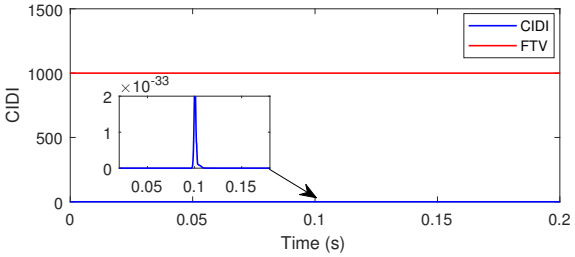

FIGURE 10. Current islanding detection indicator during LL fault event

VI. TESTING OF IDM DURING OPERATIONAL EVENTS: SIMULATION RESULTS

The simulation results for testing the IDS to identify operational conditions and discriminate such events from the islanding events are discussed in this section.

1) Switching of Capacitor

The capacitor bank of rating $600kVAr$ integrated on node 675 of test utility grid is disconnected at 2^{nd} cycle and again connected at 8^{th} cycle to realize the capacitor operational condition. The current signal associated with phase-A captured on node 650 of test network during the event of capacitor operation is recorded and illustrated in Fig. 11 (a). It is seen that due to occurrence of capacitor operation the small magnitude transients are introduced with the current signal. Magnitude of these transients is high at the time of reconnection of capacitor compared to disconnection of capacitor. This current signal is processed applying the proposed IDS and CIDI is obtained which is illustrated in Fig. 11 (b). Fig. 11 (b) details that peak magnitudes of CIDI are 1.4×10^{-9} and 5×10^{-4} at the time of disconnection and reconnection of the capacitor respectively. These peaks of CIDI are lower compared to the FTV, which indicates that capacitor bank operation is a non-islanding event of category-I. Hence, capacitor bank operation is discriminated from the islanding events and categorized as non-islanding category-I event.

2) Switching of Inductive Load

The inductive load rated at $843kW$ and $462kVAr$ and connected on node 675 of test utility grid is disconnected at 2^{nd} cycle and again connected at 8^{th} cycle to realize inductive load operational condition. The current signal associated to

This article has been accepted for publication in a future issue of this journal, but has not been fully edited. Content may change prior to final publication. Citation information: DOI 10.1109/ACCESS.2021.3092971, IEEE Access

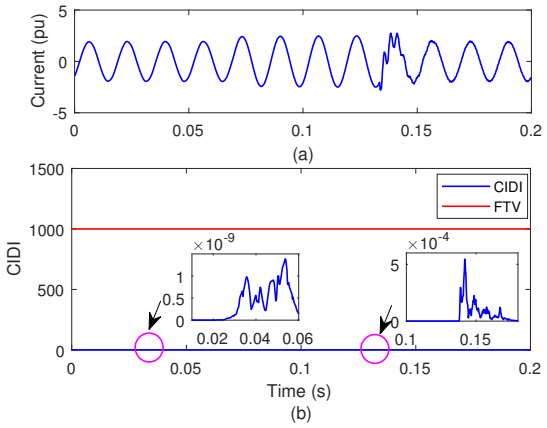

FIGURE 11. Identification of capacitor bank operation event (a) current signal associated to phase-A (b) current islanding detection indicator

phase-A captured on node 650 of test grid for the event of inductive load operation is processed applying the IDS and CIDI is obtained which is illustrated in Fig. 12. Fig. 12 details that peak magnitudes of CIDI are 2.3×10^{-29} and 6.4×10^{-23} at the time of disconnection and reconnection of the inductive load, respectively. These peaks of CIDI are lower compared to the FTV, which indicates that inductive load operation is a non-islanding event of category-I. Hence, inductive load operation event is discriminated from the islanding events and categorized as non-islanding category-I event.

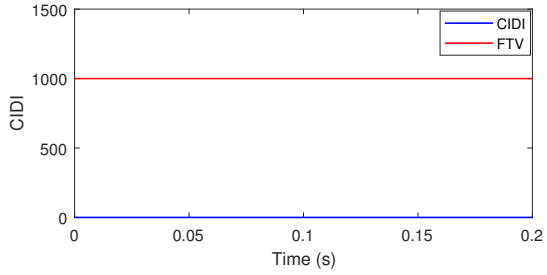

FIGURE 12. Current islanding detection indicator during inductive load operation event

3) Outage of Wind Plant

The WPP outage event is simulated at 6^{th} cycle by disconnecting the WPP from node 680 of test utility grid. The current signal associated with phase-A captured on node 650 of test grid during the event of WPP outage operation is recorded and described in Fig. 13 (a). It is viewed that due to incidence of WPP outage the current magnitude has increased. This current signal is processed applying the IDS and CIDI is obtained, which is illustrated in Fig. 13 (b). Fig. 13 (b) details that peak magnitude of CIDI is 5×10^{-3} at the time of disconnection of WPP. This peak of CIDI is lower compared to the FTV, which indicates that WPP outage event is a non-islanding event of category-I. Hence, WPP outage event is discriminated from the islanding events and categorized as non-islanding category-I event.

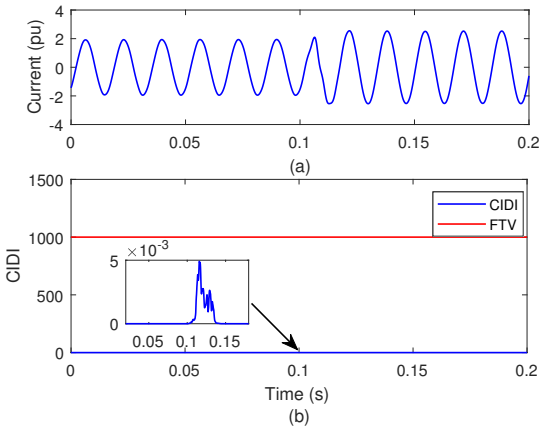

FIGURE 13. Identification of capacitor WPP outage event (a) current signal associated to phase-A (b) current islanding detection indicator

4) Outage of Solar PV Plant

The SPP outage event is simulated at 6^{th} cycle by disconnecting the SPP from node 680 of test utility grid. The current signal associated with phase-A captured on node 650 of test grid during the event of SPP outage operation is processed applying the IDS and CIDI is obtained, which is detailed in Fig. 14. Fig. 14 details that peak magnitude of CIDI is 1.4×10^{-6} at the time of disconnection of SPP. This peak of CIDI is lower compared to the FTV that indicates that SPP outage event is a non-islanding event of category-I. Hence, SPP outage event is discriminated from the islanding events and categorized as non-islanding category-I event.

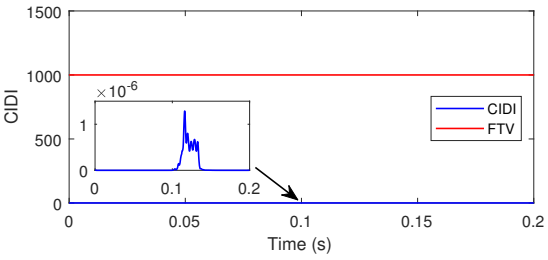

FIGURE 14. Current islanding detection indicator during SPP outage event

5) Outage of Both WPP and SPP Simultaneously

The simultaneous outage of WPP & SPP is simulated at 6^{th} cycle by disconnecting both the WPP & SPP from node 680 of test utility grid. The current signal associated with phase-A captured on node 650 of test grid during event of the simultaneous outage of WPP & SPP is processed applying the IDS and CIDI is obtained, which is detailed in Fig. 15. Fig. 15 details that peak magnitude of CIDI is 1.432 at the time of disconnection of both WPP & SPP simultaneously. This peak of CIDI is lower compared to the FTV, which indicates that simultaneous outage of WPP & SPP event is non-islanding event of category-I. Hence, simultaneous outage of WPP and SPP event is discriminated from the

This article has been accepted for publication in a future issue of this journal, but has not been fully edited. Content may change prior to final publication. Citation information: DOI 10.1109/ACCESS.2021.3092971, IEEE Access

islanding events and categorized as non-islanding category-I event.

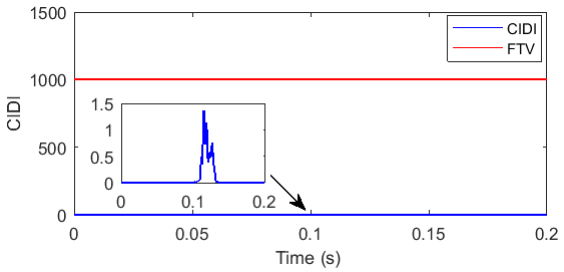

FIGURE 15. Current islanding detection indicator during simultaneous outage of WPP & SPP event

6) Grid Synchronization of both WPP and SPP Simultaneously

The event of simultaneous grid synchronization of WPP & SPP is realized at 6^{th} cycle by connecting both the WPP & SPP to node 680 of test utility grid at the same time. The current signal associated with phase-A captured on node 650 of test grid during the event of simultaneous outage of WPP & SPP is detailed in Fig. 16 (a). It is seen that transient components are associated with the event of simultaneous grid synchronization of WPP & SPP. The current signal is processed applying the IDS and CIDI is obtained which is illustrated in Fig. 16 (b). Fig. 16 (b) details that the peak magnitude of CIDI is 2.48×10^{-57} at the time of grid synchronization of both the WPP & SPP, simultaneously. The peak of CIDI is lower compared to the FTV, which indicates that simultaneous grid synchronization of WPP & SPP event is a non-islanding event of category-I. Hence, simultaneous grid synchronization of WPP & SPP event is discriminated from the islanding events and categorized as non-islanding category-I event.

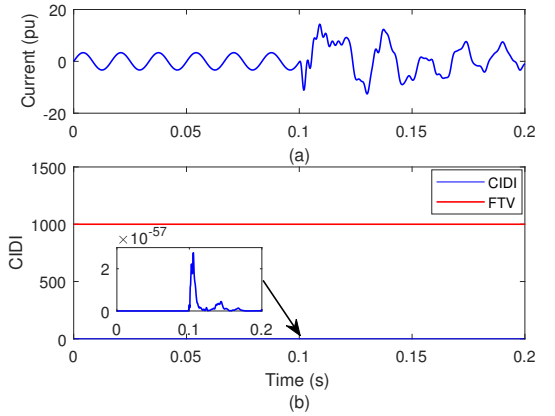

FIGURE 16. Identification of simultaneous grid synchronization of WPP & SPP event (a) current signal associated to phase-A (b) current islanding detection indicator

VII. CATEGORIZATION OF EVENTS

Maximum magnitude of the CIDI obtained by application of IDS during the islanding and non-islanding events is included in Table 6. These maximum magnitudes of CIDI are used to design the decision rules for categorization of events in three categories of islanding, non-islanding events of category-I and non-islanding events of category-II. Decision rules used for categorization of events in different categories are described in Fig. 2. The events for which the decision rule CIDI <FTV is satisfied are considered as the category-I non-islanding events. Further, the events which follows the decision rule CIDI >STV are included in the category-II non-islanding events. The events that follow the decision rule of FTV<CIDI<STV are the islanding events in the presence of WPP, SPP or both the WPP & SPP.

TABLE 6. Maximum Magnitude of CIDI

S. No.	Type of Event	Peak Magnitude
1	Islanding with WPP & SPP	3.92×10^{4}
2	Islanding with WPP	3.98×10^{4}
3	Islanding with SPP	5.42×10^{4}
4	LLLG fault	1.63×10^{-53}
5	LG fault	1.82×10^{17}
6	LLG fault	1.24×10^{17}
7	LL fault	2×10^{-33}
8	Capacitor bank operation	5×10^{-4}
9	Inductive load operation	6.4×10^{-23}
10	WPP outage event	1.4×10^{-4}
11	SPP outage event	1.4×10^{-6}
12	SPP & WPP outage at same time	1.432
13	SPP & WPP grid synchronization	2.48×10^{-57}

VIII. PERFORMANCE OF IDS

The effectiveness of IDS is evaluated in noisy and noise free environment for identification of 80 events in the noise free environment and 80 events in the noisy environment of 20 dB SNR noise level as detailed in Table 7. These different events are realized by changing the active power mismatch, reactive power mismatch, different levels of RE generation, fault incidence angles, fault impedances, fault locations, different magnitudes of capacitive and inductive loads. Table 7 describes the accurately identified, inaccurately identified and the efficiency of identification. It is established that all the events have been identified and categorized effectively with accuracy of 100% in noise free environment. In noisy environment of $20dB$ SNR, the events have been identified and categorized with an accuracy higher than 98%.

IX. REAL TIME VALIDATION OF IDS

This section details results of performance validation of the proposed current based IDS on a practical distribution network and using a real time digital simulator (RTDS).

A. PRACTICAL DISTRIBUTION NETWORK

The proposed IDS is tested for recognizing the islanding conditions realized on practical distribution feeder in the

This article has been accepted for publication in a future issue of this journal, but has not been fully edited. Content may change prior to final publication. Citation information: DOI 10.1109/ACCESS.2021.3092971, IEEE Access

TABLE 7. Efficiency of IDS for Identification of Islanding and Non-islanding Events

S. No.	Nature of event	Number of investigated events		Number of accurately categorized events		Efficiency (%)	
		Noise free	20 dB SNR noise	Noise free	20 dB SNR noise	Noise free	20 dB SNR noise
1	Islanding	18	18	18	17	100	100
2	Faults	36	36	36	35	100	97.22
3	Capacitor and load switching	16	16	18	18	100	100
4	Grid integration and outage of RE generators	10	10	10	10	100	100
	Total	80	80	100	79	100	98.75

western Rajasthan of India. The distribution feeder considered for the study is rated at 33 kV and emanated from a 132 kV grid sub-station (GSS). This 132 kV GSS has total transformation capacity of 50 MVA, 132/33 kV. The load details and RE integrated to this feeder is provided in Table 8. Four SPP with capacities of $500kW$, $200kW$, $300kW$ and $80kW$ contributes total generation of $1.08MW$. Further, two WPP each of capacity $500kW$ contributes total generation of $1MW$. This feeder is manually tripped from sending terminal at 132 kV GSS and current is captured. This current signal is processed using IDS and CIDI is computed. Peak magnitude of CIDI is found to be equal to 7.18×10^6 which is less than the STV and greater than FTV. Hence, proposed IDS has effectively identified the islanding events on a distribution feeder with availability of generation from both WPP and SPP .

TABLE 8. Details of Practical Distribution Feeder

S. No.	Name of parameter	Value of the parameter
1	Solar power plants including rooftop Solar PV	1.08 MW
2	Wind power plant	1 MW
3	Total load connected to feeder	7.04 MW

B. REAL TIME VALIDATION USING RTDS

Apart from validation of IDS on a part of practical distribution utility network, IDS has also been validated in real time using real time digital simulator (RTDS) of OPAL-RT. The experimental set-up used for the study is elaborated in Fig. 17. A laptop computer having the configuration with 64-bit operating system, 4 GB RAM, Intel(I) Core(TM)i5-3230M CPU@2.60 GHz processor is utilized as human interface device (HID) which communicates with the RTDS by an ether-net cable. Test distribution network of IEEE-13 node system having a Solar power plant of capacity $1MW$ and wind power plant of $1.5MW$ is designed using MATLAB 2011b on the HID and loaded on ML605 target of RTDS to simulate the islanding event in real time scenario. The current signals are recorded on the node 650 in the real time and transferred to the HID. These current signals are processed applying the IDS on the HID to compute the CIDI which is illustrated in Fig. 18. It is observed that peak magnitude of the CIDI is higher compared to FTV and STV. Hence, the islanding event in the presence of both SPP and WPP has been recognized effectively.

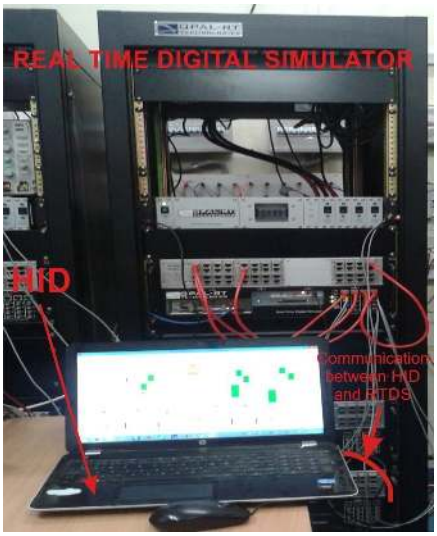

FIGURE 17. RTDS used to compute CIDI in real time scenario

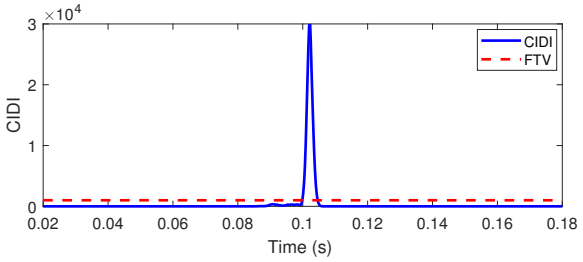

FIGURE 18. CIDI computed in real time scenario for Islanding event in the presence of solar power and wind power generation

X. PERFORMANCE COMPARISON

The performance of the proposed IDS is compared with the IDS using EMD [12], Slantlet transform and RPNN [13], ANN [14] and DWT [27]. This comparative study is performed in terms of sampling frequency, recognition time, maximum level of noise for which performance of IDS is not affected, NDZ, and RE penetration level for which study is effectively conducted. Performance comparative study is included in Table 9 where a remark on applicability of each IDS is also discussed. It is observed that proposed IDS is

least affected by the noise, effective for high RE penetration level of 50%, detects islanding in time less than $10ms$, and it has small NDZ. Further, it is also independent of nature and type of DG, and inverter/converter topology. Further, a comparative study for analysis of effect of noise on the performance fo proposed IDS and DWT based IDS reported in [27] is illustrated in Fig. 19. It is observed that proposed ST and HT based IDS effectively identify the islanding events in the noisy environment with noise level of $20dB$ compared to DWT based algorithm which identifies the islanding event effectively up to noise level of $40dB$ SNR. Performance of DWT based IDS is affected for noise level higher than $40dB$ SNR.

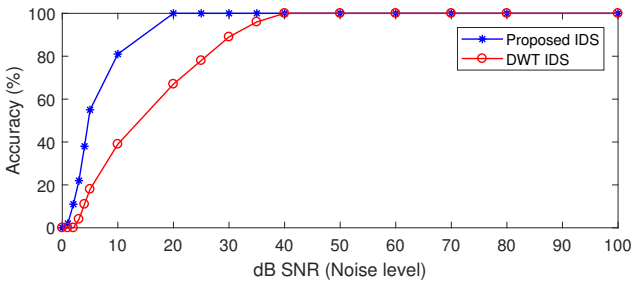

FIGURE 19. Comparative study of effect of noise on the performance of proposed IDS and DWT based IDS

XI. CONCLUSION

An islanding detection scheme is designed, which uses features extracted from current signals using hybrid combination of the ST and HT to identify and discriminate the islanding and non-islanding scenarios. A CIDI index is proposed which is computed from the factors such as SF, HF, TCF, TVF, NCF, NVF and CWF. Islanding and Non-islanding events are identified and classified by comparing the peak magnitude of CIDI with the thresholds STV and FTV. It is concluded that the proposed IDS effectively identified and categorized the islanding events, faulty and operational conditions. Decision rules making use of peak magnitude of CIDI effectively categorized the events in different categories of islanding, non-islanding category-I and non-islanding category-II. Proposed IDS effectively recognized the islanding and non-islanding conditions in the noisy environment of $20dB$ SNR with efficiency greater than 98% in a duration of less than $10ms$. Proposed IDS has minimum NDZ and it is more effective in comparison to the algorithm available in literature. IDS has been effectively tested on a practical distribution network and in real time scenario using a RTDS.

REFERENCES

[1] A. Kulshrestha, O. P. Mahela, M. K. Gupta, N. Gupta, N. Patel, T. Senjyu, M. S. S. Danish, and M. Khosravy, "A hybrid fault recognition algorithm using stockwell transform and wigner distribution function for power system network with solar energy penetration," Energies, vol. 13, no. 14, 2020.

[2] M. Ahmadipour, H. Hizam, M. L. Othman, M. A. M. Radzi, and A. S. Murthy, "Islanding detection technique using slantlet transform and ridgelet probabilistic neural network in grid-connected photovoltaic system," Applied Energy, vol. 231, pp. 645 – 659, 2018.

[3] F. Valsamas, "Comparative study of active anti-islanding schemes compatible with mics in the prospect of high penetration levels and weak grid conditions," IET Generation, Transmission Distribution, vol. 12, pp. 4589–4596(7), November 2018. [Online]. Available: https://digital-library.theiet.org/content/journals/10.1049/iet-gtd.2018.5636

[4] D. Voglitsis, F. Valsamas, N. Rigogiannis, and N. P. Papanikolaou, "On harmonic injection anti-islanding techniques under the operation of multiple der-inverters," IEEE Transactions on Energy Conversion, vol. 34, no. 1, pp. 455–467, 2019.

[5] S. Raza, H. Mokhlis, H. Arof, J. Laghari, and L. Wang, "Application of signal processing techniques for islanding detection of distributed generation in distribution network: A review," Energy Conversion and Management, vol. 96, pp. 613 – 624, 2015.

[6] S. R. Thomas, V. Kurupath, and U. Nair, "A passive islanding detection method based on k-means clustering and emd of reactive power signal," Sustainable Energy, Grids and Networks, vol. 23, p. 100377, 2020. [Online]. Available: https://www.sciencedirect.com/science/article/pii/S2352467720303088

[7] A. G. Abd-Elkader, S. M. Saleh, and M. Magdi Eiteba, "A passive islanding detection strategy for multi-distributed generations," International Journal of Electrical Power Energy Systems, vol. 99, pp. 146–155, 2018. [Online]. Available: https://www.sciencedirect.com/science/article/pii/S0142061517316058

[8] O. P. Mahela, Y. Sharma, S. Ali, B. Khan, and A. R. Garg, "Voltage-based hybrid algorithm using parameter variations and stockwell transform for islanding detection in utility grids," Informatics, vol. 8, no. 2, 2021. [Online]. Available: https://www.mdpi.com/2227-9709/8/2/21

[9] A. Pouryekta, V. K. Ramachandaramurthy, N. Mithulananthan, and A. Arulampalam, "Islanding detection and enhancement of microgrid performance," IEEE Systems Journal, vol. 12, no. 4, pp. 3131–3141, 2018.

[10] G. P. Kumar and P. Jena, "Pearson's correlation coefficient for islanding detection using micro-pmu measurements," IEEE Systems Journal, pp. 1–12, 2020.

[11] B. Wen, D. Boroyevich, R. Burgos, Z. Shen, and P. Mattavelli, "Impedance-based analysis of active frequency drift islanding detection for grid-tied inverter system," IEEE Transactions on Industry Applications, vol. 52, no. 1, pp. 332–341, 2016.

[12] A. Mohammadzadeh Niaki and S. Afsharnia, "A new passive islanding detection method and its performance evaluation for multi-dg systems," Electric Power Systems Research, vol. 110, pp. 180–187, 2014. [Online]. Available: https://www.sciencedirect.com/science/article/pii/S0378779614000200

[13] M. Ahmadipour, H. Hizam, M. L. Othman, M. A. M. Radzi, and A. S. Murthy, "Islanding detection technique using slantlet transform and ridgelet probabilistic neural network in grid-connected photovoltaic system," Applied Energy, vol. 231, pp. 645–659, 2018. [Online]. Available: https://www.sciencedirect.com/science/article/pii/S0306261918314570

[14] V. Merlin, R. Santos, A. Grilo, J. Vieira, D. Coury, and M. Oleskovicz, "A new artificial neural network based method for islanding detection of distributed generators," International Journal of Electrical Power Energy Systems, vol. 75, pp. 139–151, 2016. [Online]. Available: https://www.sciencedirect.com/science/article/pii/S0142061515003531

[15] W. H. Kersting, "Radial distribution test feeders," Power Systems, IEEE Transactions on, vol. 6, no. 3, pp. 975–985, Aug 1991.

[16] W. H. Kersting, "Radial distribution test feeders," in 2001 IEEE Power Engineering Society Winter Meeting. Conference Proceedings (Cat. No.01CH37194), vol. 2, 2001, pp. 908–912 vol.2.

[17] S. Ram Ola, A. Saraswat, S. K. Goyal, S. K. Jhajharia, B. Khan, O. P. Mahela, H. Haes Alhelou, and P. Siano, "A protection scheme for a power system with solar energy penetration," Applied Sciences, vol. 10, no. 4, 2020.

[18] R. Kaushik, O. P. Mahela, P. K. Bhatt, B. Khan, A. R. Garg, H. H. Alhelou, and P. Siano, "Recognition of islanding and operational events in power system with renewable energy penetration using a stockwell transform-based method," IEEE Systems Journal, pp. 1–10, 2020.

[19] O. P. Mahela and A. G. Shaik, "Comprehensive overview of grid interfaced wind energy generation systems," Renewable and Sustainable Energy Reviews, vol. 57, pp. 260 – 281, 2016.

[20] O. P. Mahela, B. Khan, H. H. Alhelou, and P. Siano, "Power quality assessment and event detection in distribution network with wind energy penetration using stockwell transform and fuzzy clustering," IEEE Transactions on Industrial Informatics, vol. 16, no. 11, pp. 6922–6932, 2020.

TABLE 9. Performance Comparative Study

Reference	Islanding Detection Technique	Sampling Frequency	Response Time	Maximum noise level which not affected performance of IDS (SNR)	NDZ	RE Penetration Level (%)	Remark
[12]	EMD based passive IDS	Not available	$33.33ms$	$20dB$ SNR	Small	30%	Effective for two parallel inverter based DG
[13]	Slantlet Transform and RPNN based passive IDS	$19.8kHz$	$0.17s$	$25dB$ SNR	High	10%	It is applied for single inverter based system
[14]	ANN based passive method	$7.68kHz$	$100ms$	Not investigated	Moderate	50%	Large data is required for training the ANN which increases the islanding detection time. Power quality degradation.
[27]	DWT based passive IDS	6.4 kHz	$2s$	$40dB$ SNR	High	20%	Applied for single DG
Proposed	ST+HT based passive method	$3.84kHz$	$10ms$	$20dB$ SNR	Small	50%	It is based on tracking the distortion of current waveform from sinusoidal nature. Hence, it is independent of number and type of DG. It is also independent of inverter/converter topology.

[21] O. P. Mahela and A. G. Shaik, "Comprehensive overview of grid interfaced solar photovoltaic systems," Renewable and Sustainable Energy Reviews, vol. 68, pp. 316 – 332, 2017.

[22] ——, "Detection of power quality events associated with grid integration of 100kw solar pv plant," in Energy Economics and Environment (ICEEE), 2015 International Conference on, March 2015, pp. 1–6.

[23] R. G. Stockwell, L. Mansinha, and R. P. Lowe, "Localization of the complex spectrum: the s transform," IEEE Transactions on Signal Processing, vol. 44, no. 4, pp. 998–1001, 1996.

[24] A. Derviskadic, G. Frigo, and M. Paolone, "Beyond phasors: Modeling of power system signals using the hilbert transform," IEEE Transactions on Power Systems, vol. 35, no. 4, pp. 2971–2980, 2020.

[25] E. H. Bareiss and C. P. Neuman, "Singular integrals and singular integral equations with a cauchy kernel and the method of symmetric pairing," The University of Chicago under Contract W-31-109-eng-38 with the U. S. Atomic Energy Commission, pp. 1–48, 1965.

[26] H. Samet, F. Hashemi, and T. Ghanbari, "Minimum non detection zone for islanding detection using an optimal artificial neural network algorithm based on pso," Renewable and Sustainable Energy Reviews, vol. 52, pp. 1 – 18, 2015.

[27] R. Sharma and P. Singh, "Islanding detection and control in grid based system using wavelet transform," in 2012 IEEE Fifth Power India Conference, 2012, pp. 1–4.